

Automatic Change Detection in Synthetic Aperture Radar Images Based on PCANet

Feng Gao, Junyu Dong, Bo Li, and Qizhi Xu

Abstract—This letter presents a novel change detection method for multitemporal synthetic aperture radar images based on PCANet. This method exploits representative neighborhood features from each pixel using PCA filters as convolutional filters. Thus, the proposed method is more robust to the speckle noise and can generate change maps with less noise spots. Given two multitemporal images, Gabor wavelets and fuzzy *c*-means are utilized to select interested pixels that have high probability of being changed or unchanged. Then, new image patches centered at interested pixels are generated and a PCANet model is trained using these patches. Finally, pixels in the multitemporal images are classified by the trained PCANet model. The PCANet classification result and the preclassification result are combined to form the final change map. The experimental results obtained on three real SAR image data sets confirm the effectiveness of the proposed method.

Index Terms—Change detection, Gabor wavelets, PCANet, synthetic aperture radar (SAR) images.

I. INTRODUCTION

IMAGE change detection is a process that analyzes images of the same scene taken at different times in order to identify changes that may have occurred between the considered acquisition dates. It is an important issue in both civil and military fields [1]. As for public institutions, the dynamics of natural resources are a valuable source of information in urban planning. On the other hand, for military analysts, the changes of man-made structure in airports can provide critical information in decision making.

Synthetic aperture radar (SAR) images are ideal information source for performing change detections, since they are independent of atmospheric and sunlight conditions. With the development of earth observation programs, more and more SAR sensors are capable of collecting hundreds of images for the same area on the earth's surface at shorter intervals. Therefore, SAR images are more frequently used to monitor and evaluate environmental changes. However, SAR images exhibit more difficulties than optical images due to the presence of the multiplicative speckle noise [2].

Manuscript received August 12, 2016; accepted September 7, 2016. Date of publication October 12, 2016; date of current version December 7, 2016. This work was supported in part by the National Natural Science Foundation of China under Grant 41606198, Grant 61271405, Grant 61576011, and Grant 41401174 and in part by the China Postdoctoral Science Foundation under Grant 2015M582140. (Corresponding author: Junyu Dong.)

F. Gao and J. Dong are with the Department of Computer Science and Technology, Ocean University of China, Qingdao 266100, China (e-mail: gaofeng@ouc.edu.cn; dongjunyu@ouc.edu.cn).

B. Li and Q. Xu are with the Beijing Key Laboratory of Digital Media, Beihang University, Beijing 100191, China (e-mail: boli@buaa.edu.cn; qizhi@buaa.edu.cn).

Color versions of one or more of the figures in this letter are available online at <http://ieeexplore.ieee.org>.

Digital Object Identifier 10.1109/LGRS.2016.2611001

Many methods related to the SAR image change detection have been published. Generally, SAR image change detection is composed of three main steps: 1) preprocessing, which mainly includes geometric registration or denoising; 2) difference image (DI) generation; and 3) recognition of the changed pixels and unchanged pixels. Most research works are focused on the third step. Thresholding [3], [4], clustering [5], [6], active contours [7]–[9], and Gabor feature [10] have been recently extensively studied to recognize the changed and unchanged pixels from DI. Among these methods, Li *et al.* [10] use Gabor wavelet representations to exploit the changed information. In addition, the method obtains good performance by successively implementing fuzzy *c*-means (FCM) with the nearest neighbor rule. Nevertheless, there is still room to improve if more accurate classification model is utilized.

Designing a good classification model is the most critical step in the whole change detection algorithm. Inspired by the architectural depth of the brain, deep learning has become a popular way for classification by automatically learning features from data [11], [12]. Current deep approaches always consist of multiple training stages stacked on top of each other. Each stage is generally composed of convolutional filter bank layer, nonlinear processing layer, and feature pooling layer. Restricted Boltzmann machines (RBMs) or regularized autoencoders are often involved to learn the filter bank in each stage. In the computer vision and multimedia communities, the use of deep learning is widely studied. However, in the remote sensing community, just a few change detection methods based on deep learning were presented, such as a framework based on RBM in [1] and stacked denoising autoencoders for multispatial resolution image analysis in [13]. Recently, Chan *et al.* [14] proposed PCANet, which is a simple deep learning network with its convolution filter banks chosen from PCA filters. It has demonstrated a competitive performance with other deep networks. To the best of our knowledge, a few previous works have considered PCANet for image change detection.

In this letter, a PCANet-based change detection method for multitemporal SAR images is proposed. Our main contributions are twofold.

- 1) PCANet is adopted as the classification model for change detection. PCA filters are utilized as convolutional filters; meanwhile, the hierarchical architecture of traditional convolutional neural networks is retained. These computational features have some relations to human perception and can provide discriminative power in changed and unchanged pixel classification.

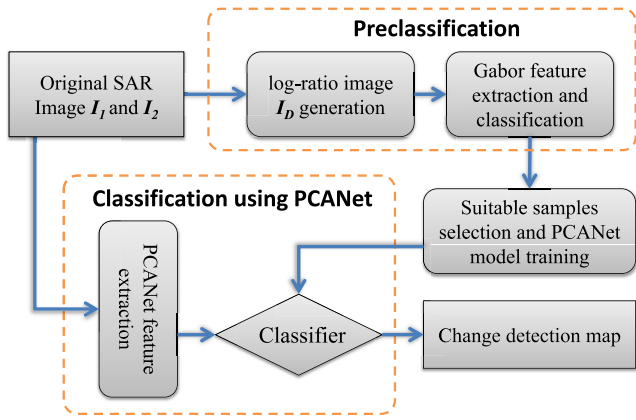


Fig. 1. Framework of the proposed change detection method.

- 2) Inspired by Li *et al.*'s work [10], a preclassification scheme is designed to obtain some labeled samples of high accuracy for PCANet using Gabor wavelets and FCM.

The FCM algorithm is implemented in a coarse-to-fine procedure to obtain enough representative samples.

The remainder of this letter is organized as follows. Section II is devoted to give problem statements and a detailed description of the proposed method. The experimental results on real multitemporal SAR images are reported in Section III. Finally, the conclusion is given in Section IV.

II. METHODOLOGY

A. Problem Statements and Overview of the Proposed Method

Given two coregistered multitemporal intensity SAR images I_1 and I_2 . The objective of change detection is to generate a change map, representing changes that occurred between the acquisition dates of two images.

The procedure of the proposed method is illustrated in Fig. 1, and is mainly composed of the following three steps.

- 1) *Step 1—Preclassification*: The log-ratio operator is used to generate the log-ratio image. Then, Gabor wavelets and FCM algorithm are utilized to select pixels if interest that have high probability of being changed or unchanged. The remaining pixels will be further classified in Step 3.
- 2) *Step 2—Training PCANet Model*: New image patches centered at interested pixels are generated. A PCANet model is trained using these patches.
- 3) *Step 3—Classification of Changed and Unchanged Pixels*: The remaining pixels in Step 1 are further separated into changed and unchanged classes using the trained PCANet model. Then, the PCANet classification result and the preclassification result are combined to form the final change map.

The detailed descriptions of Step 1 are provided in Section II-B, and the descriptions of Steps 2 and 3 are provided in Section II-C.

B. Preclassification Using Gabor Wavelets and FCM

In order to reduce the influence of speckle noise, the log-ratio operator is utilized to generate the log-ratio image I_D . It is given by $I_D = |\log(I_2/I_1)|$. Inspired by Li *et al.*'s work [10], we use Gabor wavelets to classify I_D and generate training samples for PCANet. The Gabor wavelet representation of I_D is acquired by convolving I_D with a set of Gabor kernels. In order to make a compact representation, the responses with maximum magnitude over all the possible orientations of Gabor wavelets are selected. The compact Gabor feature vector \mathbf{x} of each pixel of the log-ratio image is derived as $\mathbf{x} = [x_0, x_1, \dots, x_{V-1}]$. Thus, the Gabor features $X = [\mathbf{x}_1, \dots, \mathbf{x}_{MN}]^T$ are extracted from I_D . M and N denote the width and height of the image, respectively.

The main purpose of preclassification is to find pixels that have high probabilities of being correctly classified into changed or unchanged classes. In [10], the FCM algorithm is first performed on Gabor feature vectors to partition the log-ratio image into three clusters, respectively, denoting the changed, unchanged, and intermediate classes (i.e., w_c , w_u , and w_i). The pixels belonging to w_c and w_u have the high probability to be changed and unchanged. However, we observed that the intermediate class sometimes occupies a large part of the log-ratio image, and thus we can hardly obtain enough representative samples for PCANet training. To address this issue, we propose a novel algorithm in this section. The FCM algorithm is implemented in a coarse-to-fine procedure to restrict the proportion of intermediate class in the log-ratio image. The detailed descriptions of the proposed algorithm are as follows.

- 1) *Input*: Gabor features X corresponding to I_D .
- 2) *Step 1*: Perform the FCM algorithm on X to partition I_D into two clusters: w_c^1 and w_u^1 . The number of pixels in w_c^1 is denoted by T^1 . Then, the upper bound of real changed class is defined as $TT = \sigma \cdot T^1$. Here, σ is set as 1.20 in our implementation.
- 3) *Step 2*: Perform the FCM algorithm on X to partition I_D into five clusters: $w_1^2, w_2^2, \dots, w_5^2$. It should be noted that the five clusters are sorted by average value in descending order. To be specific, pixels in w_1^2 have the largest average value, while pixels in w_5^2 have the smallest average value. Clusters with a larger average value means that it is of higher probability to be a changed class. The number of pixels in the five clusters is defined as $T_1^2, T_2^2, \dots, T_5^2$, respectively. Set parameters $t = 1$ and $c = T_1^2$. Assign the pixels in w_1^2 to the class w_c^{pre} .
- 4) *Step 3*: Set $t := t + 1$ and $c := c + T_t^2$.
- 5) *Step 4*: If $c < TT$, assign pixels in w_t^2 to the class w_i^{pre} . Otherwise, assign pixels in w_t^2 to the class w_u^{pre} . Go to Step 3 and continue until $t = 5$.
- 6) *Output*: As a result, the preclassification change map can be denoted by an image with labels $\{w_c^{\text{pre}}, w_i^{\text{pre}}, w_u^{\text{pre}}\}$.

After preclassification, we obtain a change map with labels $\{w_c^{\text{pre}}, w_i^{\text{pre}}, w_u^{\text{pre}}\}$. The pixels belonging to w_c^{pre} have the high probability to be changed, while the pixels belonging to w_u^{pre} have the high probability to be unchanged. These two kinds of pixels can be chosen as samples. The classification

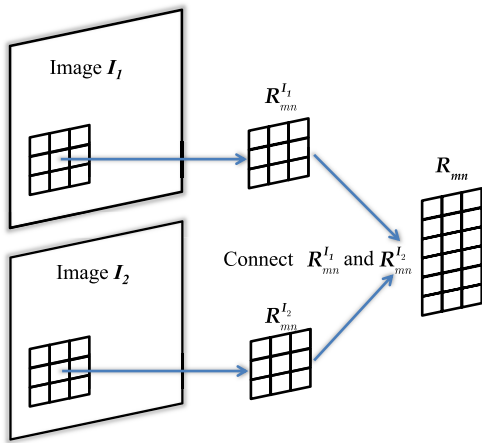


Fig. 2. Neighborhood features for each pixel as inputs.

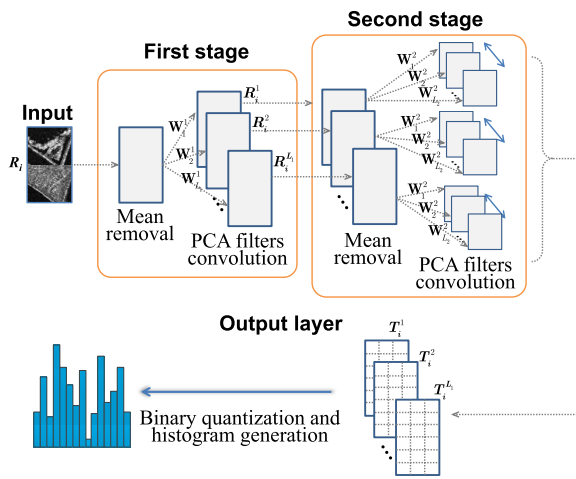


Fig. 3. Detailed block diagram of PCANet.

of pixels belonging to w_i^{pre} will be described in the following section.

C. Classification by Using PCANet

PCANet is capable of learning the nonlinear relations from multitemporal SAR images, and thus it is robust to the speckle noise. In addition, it is superior for its easy training and better adaptation to different conditions. Therefore, PCANet is utilized for change pixel classification in this letter.

The process of classification is shown in Figs. 2 and 3. First, new image patches of interested positions (pixels have high probability to belong to changed or unchanged regions) are generated, and these image patches contain enough change information around the position. As shown in Fig. 2, let $R_{mn}^{I_1}$ represent a patch with the center at position (m, n) in image I_1 and the size of $R_{mn}^{I_1}$ is $k \times k$. $R_{mn}^{I_2}$ represents the corresponding patch in image I_2 . Both patches are concatenated into a new image patch R_{mn} and the size of R_{mn} is $2k \times k$. We randomly choose N_R samples and obtain the sample images R_i , $i = 1, \dots, N_R$. Features of $\{R_i\}$ are extracted using PCANet.

The structure of PCANet is illustrated in Fig. 3. It is composed of three steps: the first two stage are PCA filter convolutions and the last stage is hashing and histogram generation. After training sample generation, we have N_R

training images of size $2k \times k$. We subtract image mean from each sample image. Then, all sample images are vectorized and combined into a matrix

$$\mathbf{Y} = [\bar{Y}_1, \bar{Y}_2, \dots, \bar{Y}_{N_R}] \in \mathbb{R}^{2k^2 \times N_R} \quad (1)$$

where \bar{Y}_i is a mean-removed vector of image R_i .

We move on to compute the eigenvectors of $\mathbf{Y}\mathbf{Y}^T$, and L_1 principle eigenvectors are selected as PCA filters. The PCA filters can be expressed as

$$\mathbf{W}_l^1 \doteq \text{mat}(q_l(\mathbf{Y}\mathbf{Y}^T)) \in \mathbb{R}^{2k^2 \times 2k^2}, \quad l = 1, 2, \dots, L_1 \quad (2)$$

where $\text{mat}(v)$ is a function that maps $v \in \mathbb{R}^{4k^4}$ to a matrix $\mathbf{W} \in \mathbb{R}^{2k^2 \times 2k^2}$ and $q_l(\mathbf{Y}\mathbf{Y}^T)$ means the l th principle eigenvector of $\mathbf{Y}\mathbf{Y}^T$. The leading principal eigenvectors capture the main variation of all the mean-removed training images. Then the l th filter output of the first stage is

$$R_i^l \doteq R_i * \mathbf{W}_l^1, \quad i = 1, 2, \dots, N \quad (3)$$

where $*$ denotes 3-D convolution. After obtaining the filter output, the first stage of the algorithm is complete.

The process of the second stage is similar to the first stage. We subtract image mean from each filtered output and collect all the l th filtered outputs to obtain $\bar{\mathbf{Z}}^l = [\bar{Z}_1^l, \bar{Z}_2^l, \dots, \bar{Z}_{N_R}^l] \in \mathbb{R}^{2k^2 \times N_R}$. After that, we combine $\bar{\mathbf{Z}}^l$ together and obtain

$$\bar{\mathbf{Z}} = [\bar{\mathbf{Z}}^1, \bar{\mathbf{Z}}^2, \dots, \bar{\mathbf{Z}}^{L_1}] \in \mathbb{R}^{2k^2 \times N_R L_1}. \quad (4)$$

The eigenvectors of $\bar{\mathbf{Z}}\bar{\mathbf{Z}}^T$ is computed and L_2 principle eigenvectors are selected as PCA filters of the second stage. For each input R_i^l of the second stage, we will have L_2 outputs, each convolves R_i^l with \mathbf{W}_l^2 for $l = 1, 2, \dots, L_2$. The number of outputs of the second stage is $L_1 L_2$. After obtaining the filter output, we finish the second stage.

At the final stage, we first binarize the filtered output of the second stage using a Heaviside step function whose value is one for positive input and zero otherwise. Around each pixel of R_i^l , the vector of L_2 binary bits can be converted into an integer value. Thus, we obtain a single integer-valued image T_i^l and every pixel of T_i^l is an integer in the range $[0, 2^{L_2} - 1]$. We further transform image T_i^l into a histogram denoted by $\text{hist}(T_i^l)$. Then, the feature of the input image R_i can be defined as

$$\mathbf{f}_i \doteq [\text{hist}(T_i^1), \text{hist}(T_i^2), \dots, \text{hist}(T_i^{L_1})]. \quad (5)$$

The extracted features from PCANet then are fed into linear SVM to train a model. Using the model, pixels belonging to w_i^{pre} are further separated into changed and unchanged classes. Finally, we combine the PCANet classification result and the preclassification result together to form the final change map.

It should be noted that the model parameters of PCANet include sample image size k , filter numbers L_1 and L_2 , and the number of stages. As mentioned in [14], inspired from the common setting of Gabor filters with eight orientations, L_1 and L_2 are always set as 8. Moreover, it is empirically verified that a two-stage PCANet is sufficient to achieve good performance. Therefore, in our implementation, we set the stage number to 2. In the training process, the training set contains about 10% of the total pixels. Moreover, we observed

that the size of sample image influences the change detection results. The analysis of the parameter will be described in detail in Section III-B.

III. EXPERIMENTAL RESULTS AND DISCUSSION

A. Experimental Setup

In order to evaluate the performance of the proposed method, we apply the proposed method to three data sets with different characteristics. The first data set is called the *Ottawa* data set, which presents a section of two SAR images acquired by an RADARSAT SAR sensor. The images present the areas where they were once afflicted with floods. The second data set is called the *San Francisco* data set. It presents a section of two SAR images acquired by an ERS-2 SAR sensor over the city of San Francisco. The third data set is called the *Yellow River* data set. It presents a section of SAR images acquired by Radarset-2 at the region of the Yellow River Estuary in China. It should be noted that the two images are a single-look image and a four-look image. Therefore, the influence of speckle noise on the second image is much greater than that of the first image. Such disparity of speckle noise aggravates the difficulties met in the process of change detection. The three data sets together with their ground-truth change maps are shown in the first three columns of Fig. 5.

Results of four other state-of-the-art techniques for change detection are given for comparison purpose. These methods are D_MRFFCM [1], PCAKM [5], MRFFCM [6], and GaborTLC [10]. These methods are implemented using the default parameters provided in [1], [5], [6], and [10], respectively. In PCAKM, $h = 5$ and $S = 3$ are used. In MRFFCM, the number of subintervals is set to 30 as mentioned in [6]. In GaborTLC, $U = 8$, $V = 5$, $k_{\max} = 2\pi$, and $f = \sqrt{2}$ are used. In D_MRFFCM, the neighborhood size is set to 5 as mentioned in [1]. The MATLAB implementation of the proposed method is available at <http://fenggao.sinaapp.com>.

The performance evaluation of SAR image change detection is a critical and basic issue. We use false alarm rate (P_{FA}), missed detection rate (P_{MD}), percentage correct classification (PCC), and Kappa coefficient (KC) as the indicators to measure the effectiveness of different methods. They are reported as percentages in the experiments. In the reference ground-truth map, the actual numbers of pixels belonging to the unchanged and changed classes are denoted by N_u and N_c , respectively. Then, $P_{FA} = FA/N_u \times 100\%$ and $P_{MD} = MD/N_c \times 100\%$, in which FA denotes the number of unchanged pixels that are detected as changed, while MD refers the number of changed pixels are detected as unchanged. The PCC is given by $PCC = (N_u + N_c - FA - MD)/(N_u + N_c) \times 100\%$. The KC gives the percentage of agreement (correct classified pixels) corrected by the number of agreements that would be expected purely by chance [10]. In addition, we compute the ratio GD/OE for quantitative evaluation, while it is given by $GD/OE = (N_c - MD)/(FA + MD)$.

B. Analysis of Parameter k

The first set of experiments is implemented on the Ottawa and San Francisco data sets to analyze the parameters' impact on the performance of the proposed method. In order to

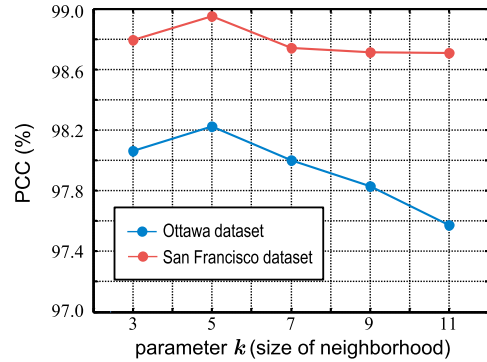


Fig. 4. Relationship between the size of neighbor and PCC on two data sets.

TABLE I
CHANGE DETECTION RESULTS OF DIFFERENT METHODS
ON THREE REAL SAR IMAGE DATA SETS

Methods	Results on the Ottawa dataset				
	P_{FA}	P_{MD}	GD/OE	PCC	KC
PCAKM [5]	1.11	9.78	5.66	97.57	90.45
MRFFCM [6]	1.90	4.60	6.29	97.69	91.27
GaborTLC [10]	0.37	12.85	5.85	97.73	90.81
D_MRFFCM [1]	1.16	4.55	8.70	98.33	93.58
Proposed method	0.85	6.93	7.98	98.22	93.06
Methods	Results on the San Francisco dataset				
	P_{FA}	P_{MD}	GD/OE	PCC	KC
PCAKM [5]	2.66	0.53	2.84	97.49	83.68
MRFFCM [6]	2.48	4.08	2.64	97.40	82.69
GaborTLC [10]	1.62	4.14	3.82	98.20	87.45
D_MRFFCM [1]	1.11	4.10	5.18	98.68	90.48
Proposed method	0.48	8.67	6.14	98.94	91.90
Methods	Results on the Yellow River dataset				
	P_{FA}	P_{MD}	GD/OE	PCC	KC
PCAKM [5]	3.51	19.83	2.24	93.54	77.85
MRFFCM [6]	1.05	22.14	2.89	95.13	82.38
GaborTLC [10]	1.90	17.21	3.20	95.33	83.68
D_MRFFCM [1]	1.08	19.92	3.23	95.51	83.92
Proposed method	3.10	10.62	3.62	95.54	85.15

generate neighborhood features for each position, we select neighborhood of size $k \times k$. The size of the neighborhood is an important parameter that can affect the final change detection results. As shown in Fig. 4, we set k to 3, 5, 7, 9, and 11 to indicate the relationship between k and PCC. The PCANet requires a neighborhood patch big enough for feature learning; if k is set as 3, the result is sensitive to neighborhood noise. Furthermore, when $k \geq 7$, the result tends to get worse, since the neighborhood features are not representative for the specified position. When k is set to 5, the proposed method achieves the best performance on both data sets. Therefore, setting $k = 5$ is the best choice. In our following experiments, we use a neighborhood of 5 pixels for feature extraction with PCANet.

C. Results and Analysis

The results of the experiments are shown and listed in Fig. 5 and Table I. The final change detection maps are shown in figure form and the criteria are shown in tabular form.

On the Ottawa data set, many slightly changed pixels are hard to detect. As shown in Fig. 5, PCAKM and GaborTLC classify these slightly changed pixels into unchanged class. It yields a high P_{MD} . On this data set, the best-known result

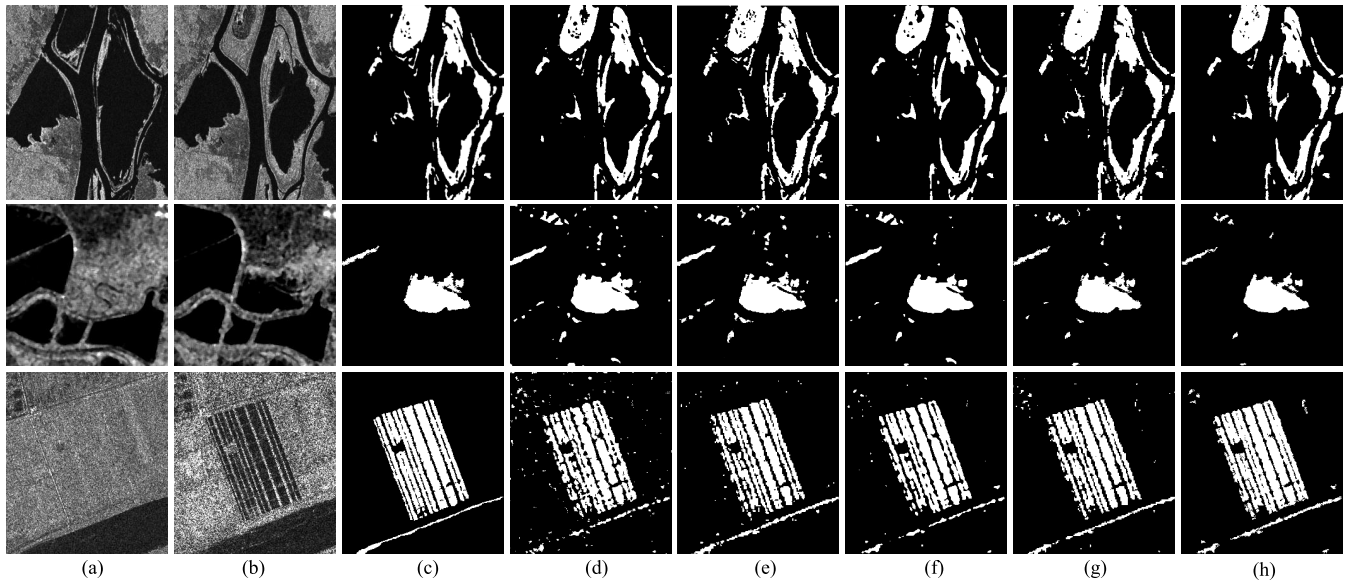


Fig. 5. Visualized results of various change detection methods on the Ottawa (first row) data set, the San Francisco (second row) data set, and the Yellow River (third row) data set. (a) I_1 . (b) I_2 . (c) Ground-truth change maps. (d) Results by PCAKM. (e) Results by MRFFCM. (f) Results by GaborTLC. (g) Results by D_MRFFCM. (h) Results by the proposed method.

is obtained by D_MRFFCM [1] with a PCC value of 98.33%. The proposed method achieves a PCC value of 98.22%, which is quite competitive to D_MRFFCM on this data set.

On the San Francisco data set, it can be observed that the proposed method performs best with the largest PCC value of 98.94%, largest GD/OE value of 6.14, and the largest KC value of 91.90%. As shown in Fig. 5, the result obtained by the proposed method exhibits less noise spots compared with other methods. It is evident that the proposed method is robust to the speckle noise by generating representative neighborhood features for each pixel using PCANet. That is why FA yielded by the proposed method is much lower.

On the Yellow River data set, the influence of speckle noise is much greater. It represents a more complicated situation to assess the effectiveness of the proposed method. As shown in Fig. 5, there are many white spots in the change map generated by other methods on the Yellow River data set. As shown in Table I, the proposed method obtains the largest GD/OE and PCC values. In addition, the value of KC of the proposed method is the best. It should be noted that the value of KC is the most cogent and discriminative criterion. The results indicate that the proposed method outperforms the other methods and is capable of improving the change detection accuracy.

IV. CONCLUSION

This letter has presented a change detection method for SAR images based on hierarchical FCM clustering and PCANet. The proposed method exploits representative neighborhood features from each pixel using PCA filters as convolution filters. Then, the proposed method is robust to the speckle noise and it yields lower false alarms. Compared with four closely related methods, the proposed method exhibits good performance. In the future, we will do research on accelerating the proposed method using parallel algorithms on GPU or detect changed point targets.

REFERENCES

- [1] M. Gong, J. Zhao, J. Liu, Q. Miao, and L. Jiao, "Change detection in synthetic aperture radar images based on deep neural networks," *IEEE Trans. Neural Netw.*, vol. 27, no. 1, pp. 125–138, Jan. 2016.
- [2] L. Jia *et al.*, "SAR image change detection based on iterative label-information composite kernel supervised by anisotropic texture," *IEEE Trans. Geosci. Remote Sens.*, vol. 53, no. 7, pp. 3960–3973, Jul. 2015.
- [3] Y. Bazi, L. Bruzzone, and F. Melgani, "An unsupervised approach based on the generalized Gaussian model to automatic change detection in multitemporal SAR images," *IEEE Trans. Geosci. Remote Sens.*, vol. 43, no. 4, pp. 874–887, Apr. 2005.
- [4] G. Moser and S. B. Serpico, "Generalized minimum-error thresholding for unsupervised change detection from SAR amplitude imagery," *IEEE Trans. Geosci. Remote Sens.*, vol. 44, no. 10, pp. 2972–2982, Oct. 2006.
- [5] T. Celik, "Unsupervised change detection in satellite images using principal component analysis and k -means clustering," *IEEE Geosci. Remote Sens. Lett.*, vol. 6, no. 4, pp. 772–776, Oct. 2009.
- [6] M. Gong, L. Su, M. Jia, and W. Chen, "Fuzzy clustering with a modified MRF energy function for change detection in synthetic aperture radar images," *IEEE Trans. Fuzzy Syst.*, vol. 22, no. 1, pp. 98–109, Feb. 2014.
- [7] Y. Bazi *et al.*, "Unsupervised change detection in multispectral remotely sensed imagery with level set methods," *IEEE Trans. Geosci. Remote Sens.*, vol. 48, no. 8, pp. 3178–3187, Aug. 2010.
- [8] T. Celik and K.-K. Ma, "Multitemporal image change detection using undecimated discrete wavelet transform and active contours," *IEEE Trans. Geosci. Remote Sens.*, vol. 49, no. 2, pp. 706–716, Feb. 2011.
- [9] H. Li, M. Gong, and J. Liu, "A local statistical fuzzy active contour model for change detection," *IEEE Geosci. Remote Sens. Lett.*, vol. 12, no. 3, pp. 582–586, Mar. 2015.
- [10] H.-C. Li, T. Celik, N. Longbotham, and W. J. Emery, "Gabor feature based unsupervised change detection of multitemporal SAR images based on two-level clustering," *IEEE Geosci. Remote Sens. Lett.*, vol. 12, no. 12, pp. 2458–2462, Dec. 2015.
- [11] B. Chen, G. Polatkan, G. Sapiro, D. Blei, D. Dunson, and L. Carin, "Deep learning with hierarchical convolutional factor analysis," *IEEE Trans. Pattern Anal. Mach. Intell.*, vol. 35, no. 8, pp. 1887–1901, Aug. 2013.
- [12] Y. Bengio, A. Courville, and P. Vincent, "Representation learning: A review and new perspectives," *IEEE Trans. Pattern Anal. Mach. Intell.*, vol. 35, no. 8, pp. 1798–1828, Aug. 2013.
- [13] P. Zhang, M. Gong, L. Su, J. Liu, and Z. Li, "Change detection based on deep feature representation and mapping transformation for multi-spatial-resolution remote sensing images," *ISPRS J. Photogram. Remote Sens.*, vol. 116, pp. 24–41, Jun. 2016.
- [14] T.-H. Chan, K. Jia, S. Gao, J. Lu, Z. Zeng, and Y. Ma, "PCANet: A simple deep learning baseline for image classification?" *IEEE Trans. Image Process.*, vol. 24, no. 12, pp. 5017–5032, Dec. 2015.